



HAL
open science

Automatic defect localization and characterization through machine learning based inversion for guided wave imaging in SHM

Roberto Miorelli, Andrii Kulakovskiy, Olivier Mesnil, Oscar D'almeida

► To cite this version:

Roberto Miorelli, Andrii Kulakovskiy, Olivier Mesnil, Oscar D'almeida. Automatic defect localization and characterization through machine learning based inversion for guided wave imaging in SHM. AIP Conference Proceedings, 2019, Volume 2102: 45th Annual Review of Progress in Quantitative Nondestructive Evaluation, 2102, pp.050005. 10.1063/1.5099771 . cea-04555919

HAL Id: cea-04555919

<https://cea.hal.science/cea-04555919>

Submitted on 23 Apr 2024

HAL is a multi-disciplinary open access archive for the deposit and dissemination of scientific research documents, whether they are published or not. The documents may come from teaching and research institutions in France or abroad, or from public or private research centers.

L'archive ouverte pluridisciplinaire **HAL**, est destinée au dépôt et à la diffusion de documents scientifiques de niveau recherche, publiés ou non, émanant des établissements d'enseignement et de recherche français ou étrangers, des laboratoires publics ou privés.

Automatic Defect Localization and Characterization Through Machine Learning Based Inversion for Guided Wave Imaging in SHM

Roberto Miorelli¹, Andrii Kulakovskiy^{1,2}, Olivier Mesnil^{1,a)}, Oscar d’Almeida²

¹ NDE department CEA LIST, Saclay, France

² Safran Tech, Magny-Les-Hameaux, France

^{a)}Corresponding author: olivier.mesnil@cea.fr

Abstract. Guided Wave (GW) based Structural Health Monitoring (SHM) relies on the permanent integration of sensors on a structure to measure propagated guided waves and deduce information regarding its current structural health. GW imaging takes advantage of the GW measurements to establish a cartography of the health of the inspected structure, leading to the detection and the localization of the possibly present defects. Characterization of the defects from the obtained maps is often not directly possible, as the size and magnitude of the defect indication depends on a substantial number of parameters beyond the defect size, such as the wavelength of interrogation or the reflectivity of the flaw. So far, characterization of defect size through guided wave imaging in SHM context has therefore only been achieved in controlled environments for well-known flaws. This communication presents the use of the GW-SHM simulation models developed at CEA-LIST to build a large database of GW imaging results and train a machine learning based inversion algorithm on it. Firstly, a training set accounting for various inspection parameters, e.g., frequency, flaw position and size is generated. Secondly, imaging algorithms are applied to each database sample and these images are used, in the so-called training phase, to build an inverse model with a supervised machine learning algorithm. In practice, this corresponds to fit a regressor (e.g., kernel ridge regressor, support vector regressor, Gaussian process regressor, etc.) on the set of signals/parameters pairs. To assess the performance of the inversion strategy, (i.e., the capability to retrieve flaw positions and/or dimensions), the inverse model is evaluated on new datasets (usually called test sets), which were generated independently from the training phase. The inversion results are analyzed with respect to accuracy and CPU time efficiency.

INTRODUCTION

Structural Health Monitoring (SHM) consists of permanently installing sensors onto or into a structure in order to continuously or periodically monitor its health in a non-destructive fashion. The main objective of SHM is to certify the health of the structure until the next maintenance operation. Guided Waves (GWs) are elastic waves guided by the structure in which they propagate and are a promising mean of interrogation to detect defects in plate-like structures. GW-based SHM (GW-SHM) has received significant interest from the scientific community and a very large number of in-lab GW-SHM prototypes have been documented.

A common application of GW-SHM is through Guided Wave Imaging (GWI) aiming at creating images representing the health of the inspected structures, for example reported in [1], [2], [3], [4]. Most often GWI relies on an array of piezoelectric (PZT) transducers, each acting sequentially as emitter and receiver of GW in order to measure the propagated wave packets between every pair of sensors. Images obtained through GWI allow for a visual interpretation to detect and roughly locate the defects. In general however, the characterization (type and size) of the defect is not directly possible based on the images.

In the recent years, machine learning (ML) algorithms are gaining the interest of the NDT&E research community as valuable tools to address challenging tasks such as automatic classification and regression [5]. In this paper, we focused our attention on the ML category known under the name of supervised learning [6] in order to invert a defect size based on images obtained through GWI. That is, with supervised learning we postulate the knowledge of input parameters (e.g., flaw(s) dimension(s), position(s), probe(s) geometrical parameter(s), etc.) and the associated inspection output/target signals. Starting from a sufficiently large collection of input parameters/output couples a

model targeting classification or regression tasks is fit on these data. This preliminary and possibly computationally expensive phase is known as training phase. Once the model is trained, starting from a set of “new” measurements, the ML algorithm enables almost real time predictions (i.e., it provides the set of input parameters which “are behind” the measured signals). This phase is also called on-line phase. In this paper, we study the performance of different classification and regression algorithms trained by employing CIVA SHM forward solver [7] where signals were post-processed via the Excitelet algorithm [8]. Moreover, different excitation frequencies have been considered in order to assess the classification and regression performance at various inspection frequencies.

GUIDED WAVE IMAGING

Imaging process

Guided Waves Imaging (GWI) is one of the most effective approaches to evaluate the integrity of a structure. A spatially distributed array of piezoelectric transducers is considered for both actuating and sensing the propagating guided waves. Collected signals are then processed by the defect imaging algorithm in order to construct a cartography, where each pixel is mapped to the corresponding elementary portion of the structure. The damage presence and location are deduced by analyzing the spatial intensity distribution of the cartography. However, the size of the defect is not directly proportional to the dimensions of the indication representing the defect on the cartography.

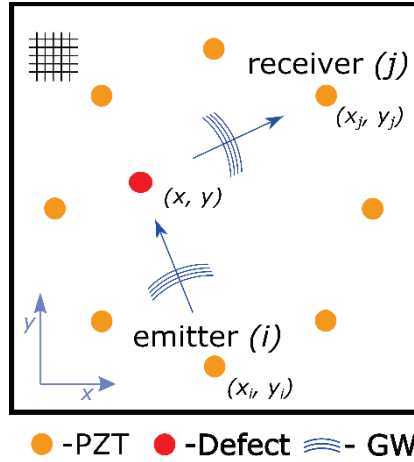


Figure 1: Illustration of GWI methodology for defect cartography computation. GWs are excited and measured by the sparse grid of the PZTs distributed over the structure.

A schematic of the GWI process is represented in **Figure 1**. The grid of pixels discretizes the region of interest of the studied specimen. In the current study, we use a baseline algorithm, named Excitelet, which attributes a global Damage Index (DI) value to each pixel. Exploiting the GW propagation specifications, it processes residual signals that are measured by each pair of piezo-electric transducers distributed over the structure. It is also assumed that the wavelength of the excited GW is of the same order of magnitude as the defect size in order to observe GW’s diffraction effects. Therefore, the residual signal, obtained as the difference between pristine and damaged states of the structure, contains echoes coming from the defect.

Aforementioned, global DI value (1) is obtained as the sum of the local DI_j (2) values computed for each PZT j^{th} pair [8]. The latter is expressed via the modulus of a correlation coefficient between the experimental residual and theoretical signal propagated from the emitter to the point of interest and on to the receiver.

$$DI(x_i, y_i) = \sum_j DI_j(x_i, y_i) \quad (1)$$

$$DI_j(x_i, y_i) = \left| \frac{\int_{t_0}^{t_{max}} S_{emit_j \rightarrow rec_j}^{exp}(t) S_{emit_j \rightarrow rec_j}^{theor}(t) dt}{\sqrt{\int_{t_0}^{t_{max}} \left(S_{emit_j \rightarrow rec_j}^{exp}(t) \right)^2 dt \int_{t_0}^{t_{max}} \left(S_{emit_j \rightarrow rec_j}^{theor}(t) \right)^2 dt}} \right|, \quad (2)$$

where $DI(x_i, y_i)$ denotes damage index value for a (x_i, y_i) pixel, $S_{emit_j \rightarrow rec_j}^{exp}(t)$ denotes the experimental residual signal and $S_{emit_j \rightarrow rec_j}^{theor}(t)$ denotes the theoretical signal for the corresponding PZT pair. The theoretical signal can be calculated as a convolution of an excitation function with the Green's function (3) that describes the GW propagation in the structure of interest:

$$S_{emit \rightarrow rec}^{theor}(r, t) = u(t) * G_{emit \rightarrow obs}(r_1, t) * G_{obs \rightarrow rec}(r_2, t), \quad (3)$$

where $u(t)$ denotes excitation function, $G(r, t)$ is the Green's function, r_1 and r_2 denote the distances from an emitter to an observation point and to a receptor respectively.

Database creation

To apply ML methodologies, large datasets are required. In our case, it means that a large number of Excitelet images must be constructed and fed to the ML process, with varying parameters. As creating hundreds of experimental cases leads to a prohibitive cost, simulation was used to simulate the studied configuration. The CIVA software with the SHM package [9] was used in order to create a large database in a reasonable computation time. Typically for the studied aluminum panel with 8 transducers and a through hole, the whole process (simulation of the 8 guided wave propagation, extraction of the data, Excitelet application) took between 4 to 10 minutes, depending on the frequency, for each image. The validation of this software on a case similar to the one presented in this paper, as well as its performances were discussed in the companion paper [10].

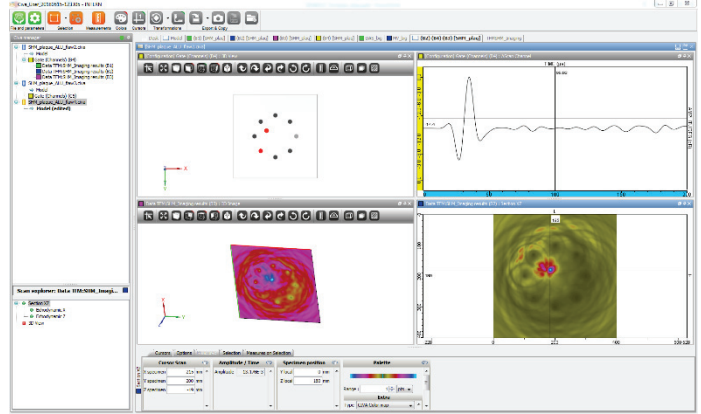
MACHINE LEARNING BASED INVERSION

Presentation of the configuration

In the following subsection we detail a general framework adopted for training ML algorithms and testing their performances in the context of a SHM inspection problems for both classification and regression tasks. More into details, we assume that a sufficiently large set of labeled data are available either by employing synthetic signals or by employing directly experimental measurements. The test case considered for classification and regression tasks deals with an aluminum plane layer of size $600 \times 600 \times 3$ mm³ flawed by a hole with a radius ranging from 2.5 mm up to 7.5 mm. We suppose that the flaw can take up any positions on the plate within a zone surrounded by eight evenly spaced piezoelectric sensors laying on a circumference having 300 mm in diameter (e.g., see Figure 2). Three different frequencies, e.g., 20 kHz, 40 kHz and 60 kHz have been considered in our simulations.



(a)

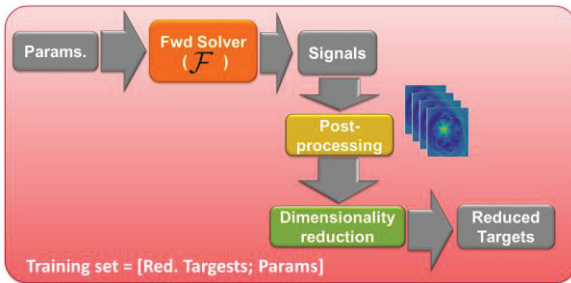


(b)

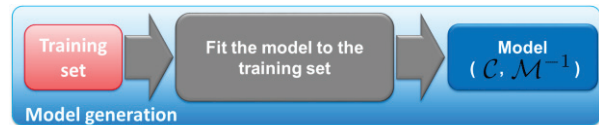
Figure 2. In (a) the studied configuration and in (b) an example of the numerical counterpart simulated via CIVA SHM module.

Training phase

In this paper, we perform the training phase by generating a database of synthetic signals based on CIVA SHM forward solver [10] then the signals are post-processed by using Excitelet algorithm [8] [4]. More into details, we have run CIVA SHM forward solver for different values of flaw position along x and y as well as different flaw radius. The three dimension parameters space have been sampled by collecting $N=500$ samples based on a Latin Hypercube Sampling (LHS) design. Then, the Excitelet algorithm has been applied to the synthetic signals in order to obtain the associated maps having size 600×600 pixels each. That is, we have built a database of $500 \times 600 \times 600$ labelled data which we refer hereafter under the name of training set. In order to avoid the so-called curse-of-dimensionality problem, we extracted the most meaningful feature from the training set by employing the Principal Component Analysis (PCA) algorithms [2]. As a consequence the training set size shrunk down to a more suitable 500×10 set of real values, this procedure have been schematically shown in **Figure 3a**. Once the training set is created, one wants to fit (i.e., generate) a model on it able to perform a dedicated task. In this work, we focused our attention on both classification (C) and regression (M^{-1}) tasks (see Fig. **Figure 3b**) as detailed in the next two subsections.



(a)



(b)

Figure 3. Block diagram of (a) the training set generation phase and (b) the one associated to the model generation targeting classification or regression tasks.

Classification

As previously mentioned, we have considered that the training set generation phase provide a labelled set of data containing input parameters and extracted features. The extracted features have been obtained from a set of N sets of guided wave signals that have been post-processed with the Excitelet algorithm. Subsequently, the obtained N maps have been treated with PCA algorithm in order to project these maps into a much lower dimensional space that

represents the space of reduced targets. The aforementioned chain of operations dealing with the creation of the training set is sketched in **Figure 4**.

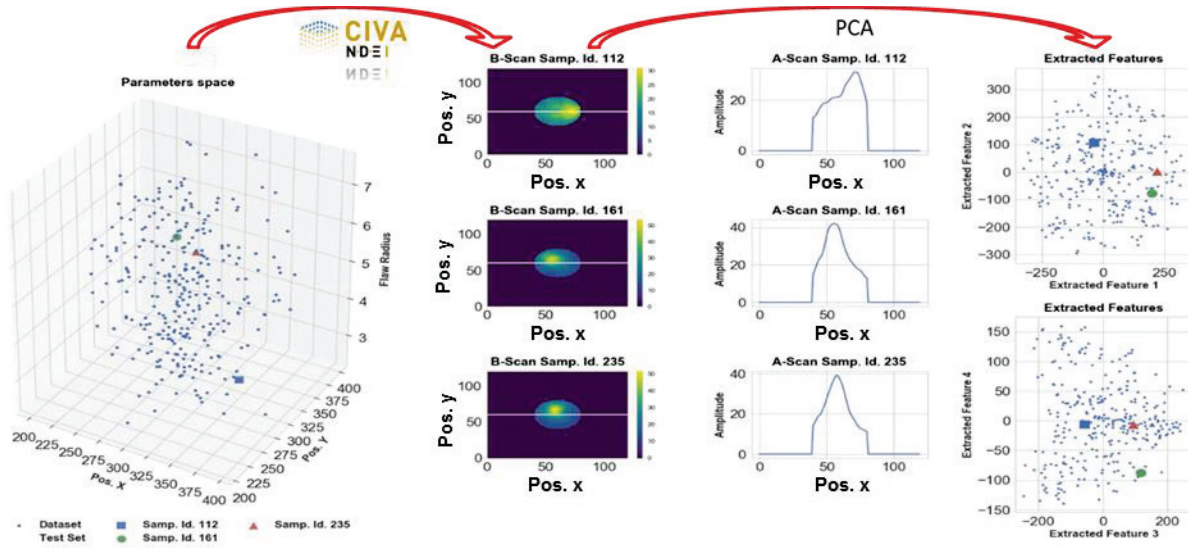


Figure 4. From left to right we sketch the set of operation we performed in the training phase targeting classification and regression tasks. On the left, we show the set of parameters generated via LHS design, which have been employed to feed CIVA SHM solver. In the middle, the maps obtained via Excitelet algorithm and the associated projected signals in the PCA space on the right.

In this paper, we have focused our attention onto the classification algorithms known in the literature as Naïve Bayes (NB) and Support Vector Classification (SVC) [5] [11] [12]. The targeted classes were chosen with respect to the hole radius regardless of the position taken up by the hole in the metallic plate. The data labelled with Class 1 represent all the hole with radius larger than 6.0 mm. Within the Class 2 we have gathered the holes having radius between 6.0 mm and 4.0 mm whereas the Class 3 defines all the holes having radius smaller than 4.0 mm. The SVC model with Gaussian kernel has been fit on the training set by employing a 5-folds cross validation procedure.

In order to study the influence of the frequency on the classification accuracy, we tested both the algorithms at the frequencies of 20 kHz, 40 kHz and 60 kHz. For each frequency, a test set composed of 200 samples have been generated via LHS design and then simulated by using CIVA SHM solver. In Fig. 4, by employing confusion maps, we displayed the classification results obtained via NB and SVC classifiers. These results shown that the classifiers provide almost the same performance and that the classification accuracy degrade when the frequency increase.

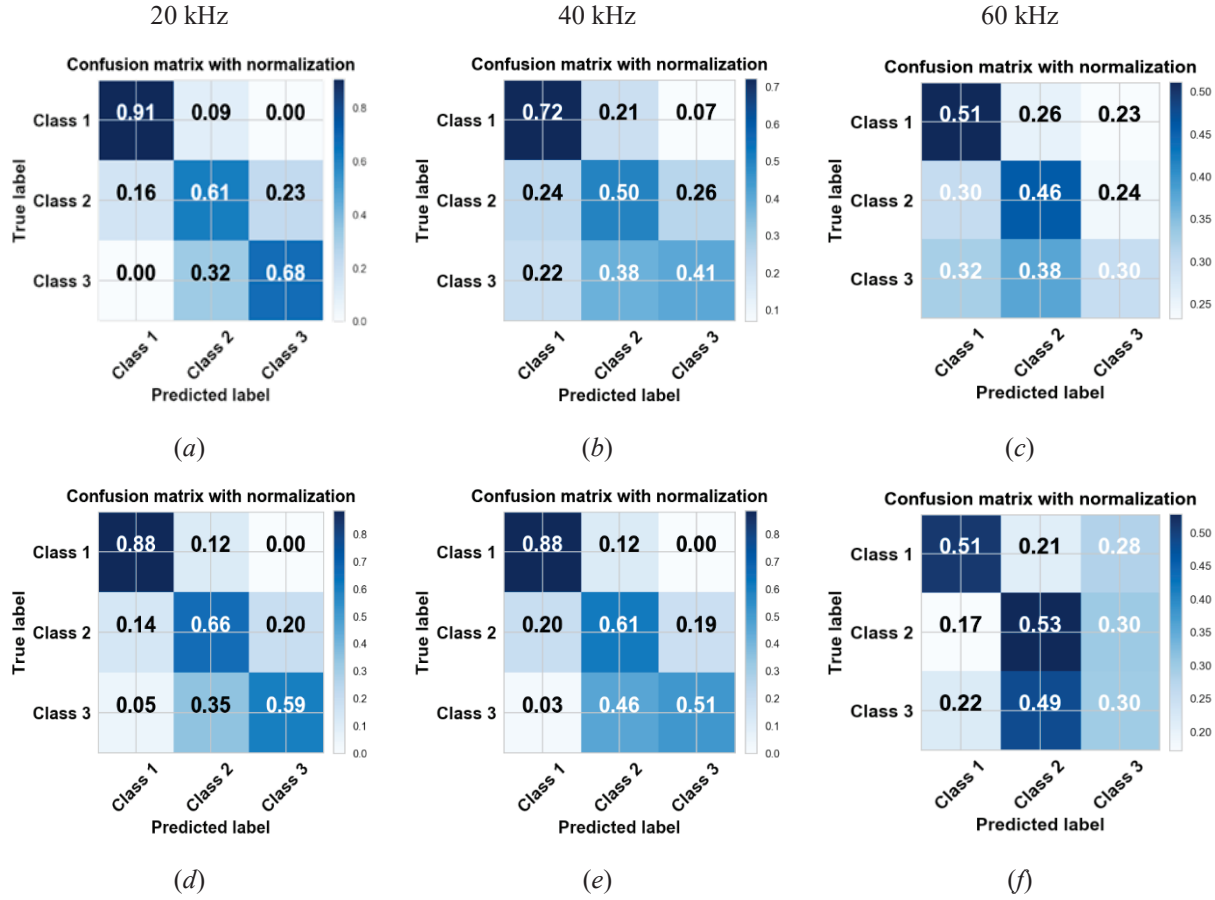


Figure 5. Classification results obtained at 20 kHz, 40 kHz and 60 kHz shown through (normalized) confusion matrices. Naïve Bayes classification results are shown in (a), (b) and (c) whereas the SVC results are displayed in (d), (e) and (f).

Regression

In order to train a regressor algorithm targeting inversion tasks, we generated a training set made of 500 samples based on LHS design, we applied PCA feature extraction on the Excitelet maps as shown in Fig. 4. To perform regression tasks aiming to retrieve flaw x and y positions and the hole radius values, we fit a Kernel Ridge Regression (KRR) regressor [6] on the training set. More in particular, a 5-folds cross validation stage has been employed to fit the KRR model with Gaussian kernel to the training set. Subsequently, we tested the obtained results on a test set composed by 200 samples generated via LHS design. In Fig. 5 we shown prediction obtained via KRR regressor based on synthetic test set. By looking at the obtained prediction one can readily notice that the overall accuracy of KRR prediction is quite good concerning flaw x and y positions since the scattered plots fit well the 45° black solid line when the two highest frequencies are addressed. Slightly worst results have been obtained at 20 kHz though. Concerning the prediction of flaw radius, an opposite behavior was found since the best results are provided by the frequencies of 20 kHz and 40 kHz.

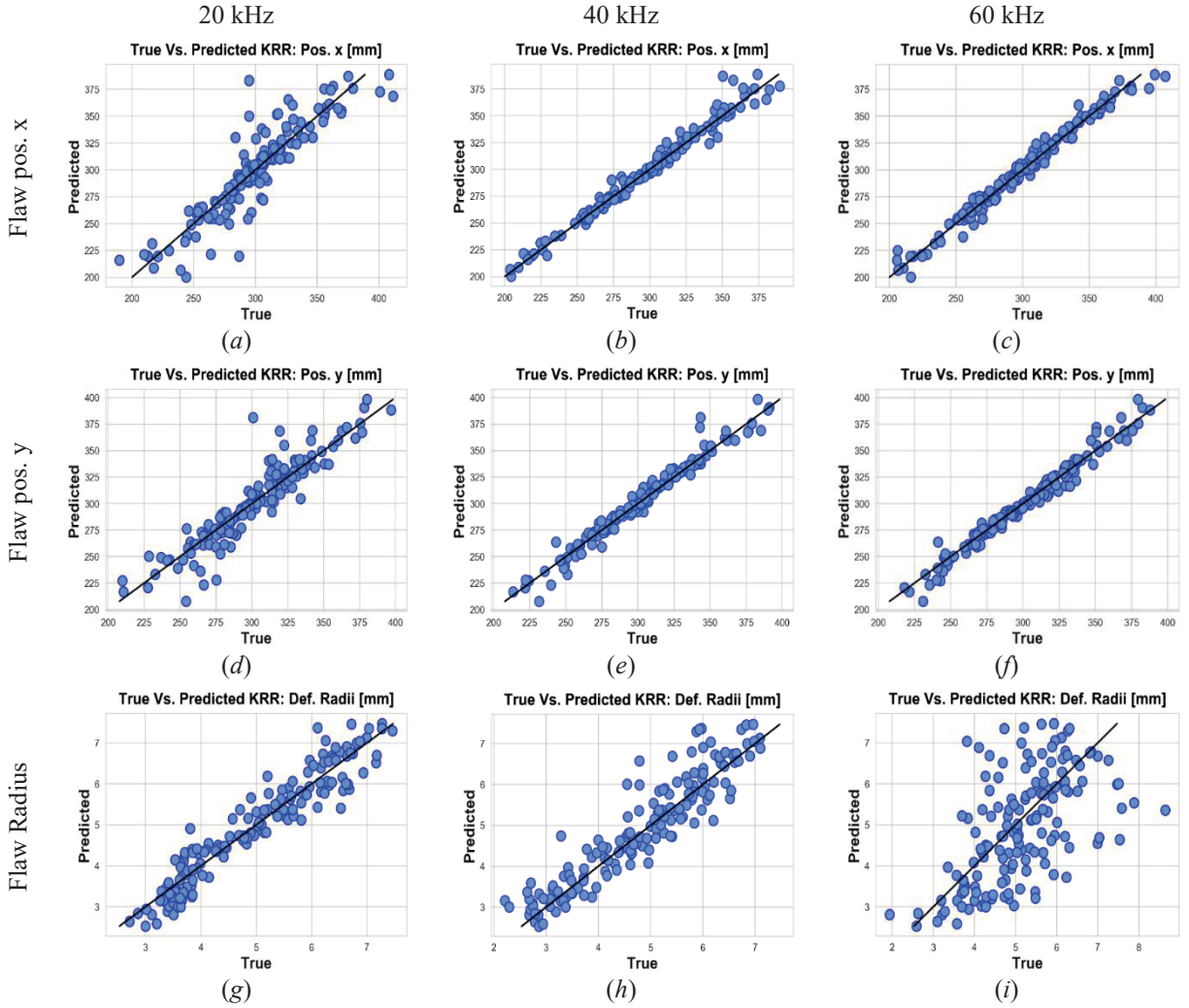


Figure 6. KRR predictions are shown via true vs. predicted curves. In (a), (b) and (c) KRR results are provided for flaw position in the x direction and in (d), (e) and (f) prediction associated to flaw positions along y are given at 20 kHz, 40 kHz and 60 kHz, respectively. In (g), (h) and (i) we displayed, in the order, KRR hole radius predictions for the three frequencies considered before.

CONCLUSION

This article presents the results of classification and inversion of a defect size based on data of Guided Wave Imaging. The database contains 500 images corresponding to the Excitelet algorithm applied to an aluminum panel drilled by a circular through-hole of various positions and diameters. Approximately 350 images were used for the training while 150 were used to evaluate the quality of the classifier and regressor. Overall, the classification provides mitigated results, mainly because the classes of defect were arbitrarily determined and no true distinction existed between the classes. Future work on classification will include looking a very distinct classes, for example one class per number of defect in the inspected structure. On the regression side, the results were much more satisfying, for example the defect size was inverted with a mean absolute error of about 0.3 mm at 40 kHz, meaning that the approach is viable to inverse defect size.

REFERENCES

- [1] X. Zhao, H. Gao, G. Zhang, B. Ayhan, F. Yan, C. Kwan and J. L. Rose, "Active health monitoring of an aircraft wing with embedded piezoelectric sensor/actuator network: I. Defect detection, localization and growth monitoring," *Smart materials and structures*, vol. **16**(4), p. 1208, (2007).
- [2] J. E. Michaels, "Detection, localization and characterization of damage in plates with an in situ array of spatially distributed ultrasonic sensors," *Smart Materials and Structures*, vol. **17**(3), p. 035035,(2008).
- [3] J. S. Hall and J. E. Michaels, "Minimum variance ultrasonic imaging applied to an in situ sparse guided wave array," *IEEE transactions on ultrasonics, ferroelectrics, and frequency control*, vol. **57**(10), pp. 2311-2323, (2010).
- [4] A. Kulakovskiy, B. Chapuis, O. Mesnil, N. Bedreddine, O. D'Almeida and A. Lhemery, "Defect imaging on CFRP and honeycomb composite structures by guided waves generated and detected by a sparse PZT array," *Structural Health Monitoring 2017*, (2017).
- [5] M. Salucci, N. Anselmi, G. Oliveri, P. Calmon, R. Miorelli, C. Reboud and A. Massa, "Real-time NDT-NDE through an innovative adaptive partial least squares SVR inversion approach," *IEEE Transactions on Geoscience and Remote Sensing*, vol. **54**(11), pp. 6818--6832, (2016).
- [6] C. M. Bishop, *Pattern recognition and machine learning*, 2006.
- [7] O. Mesnil, A. Imperiale, E. Demaldent, V. Baronian and B. Chapuis, "Simulation tools for guided wave based structural health," *AIP Conference Proceedings*, vol. **1949**, p. 050001, (2018).
- [8] N. Quaegebeur, P. Masson, D. Langlois-Demers and P. Micheau, "Dispersion-based imaging for structural health monitoring using sparse and compact arrays," *Smart Materials and Structures*, vol. **20**(2), p. 025005, (2011).
- [9] Extende, "CIVA in a few words," [Online]. Available: <http://www.extende.com/civa-in-a-few-words>. [Accessed August 2018].
- [10] O. Mesnil, A. Imperiale, E. Demaldent and B. Chapuis, "Validation of spectral finite element simulation tools dedicated to guided wave based Structural Health Monitoring," *AIP Conference Proceedings*, 2019.
- [11] S. Ahmed, R. Miorelli, C. Reboud, P. Calmon, N. Anselmi and M. Salucci, "Fast Characterization of Multiple Cracks in Conductive Media based on Adaptive Feature Extraction and SVR," *Series Studies in Applied Electromagnetics and Mechanics Ebook Volume 43: Electromagnetic Non-Destructive Evaluation (XXI)*, p. 191 – 198, 2018.
- [12] S. Ahmed, R. Miorelli, C. Reboud, P. Calmon, N. Anselmi, M. Salucci and A. Massa, "Real time flaw detection and characterization in tube through partial least squares and SVR: Application to eddy current testing," *AIP Conference Proceedings*, p. 020026, 2018.